Ab initio molecular dynamics study of water oxidation reaction pathways in mono-ru catalysts

Valles-Pardo, J.L.; Guijt, M.C.; Iannuzzi, M.; Joya, K.S.; Groot, H.J.M. de; Buda, F.

CHEMPHYSCHEM

DOI: 10.1002/cphc.201100546

Ab Initio Molecular Dynamics Study of Water Oxidation Reaction Pathways in Mono-Ru Catalysts

José Luis Vallés-Pardo,[a] Marieke C. Guijt,[a] Marcella Iannuzzi,[b] Khurram S. Joya,[a, c] Huub J. M. de Groot,[a] and Francesco Buda*[a]

Ab initio molecular dynamics simulations with an adaptive biasing potential are carried out to study the reaction path in mononuclear Ru catalysts for water oxidation of the type $[(Ar)Ru(X)(bpy)]^+$ with different aromatic ligands (Ar). The critical step of the O–O bond formation in the catalytic cycle starting from the $[(Ar)Ru(O)(bpy)]^{2+}$ intermediate is analyzed in detail. It is shown that an explicit inclusion of the solvent environment is essential for a realistic description of the reaction path. Clear evidence is presented for a concerted reaction in which the O–O bond formation is quickly followed by a proton transfer leading to a Ru–OOH intermediate and a hydronium ion. An alternative path in which the approaching water first coordinates to the metal centre is also investigated, and it is found to induce a structural instability of the catalyst with the breaking of the aromatic ligand coordination bond.

1. Introduction

One of the most important processes in natural and artificial photosynthesis is water oxidation in which water is split into O_2 and H_2.[1] Taking inspiration from the natural Mn based oxygen evolving complex in photosystem II, a large effort in the last decades has been devoted to synthesize transition metal complexes which could perform the same activity. A microscopic mechanistic understanding of the natural process is clearly relevant to support the design of artificial devices for fuel generation from solar energy.[2,3] The most successful artificial catalysts are based on Ru,[4,5] Co,[6–8] and more recently Ir complexes.[9] In particular, mononuclear molecular catalysts based on Ir^{III} have shown to be highly active and robust.[10–12] Density functional theory (DFT) calculations have been also performed to clarify the underlying reaction mechanism in some of these catalysts.[10,11,13–15] Available computational chemistry tools have in our view reached a predictive power which is good enough to allow not only the understanding of reaction mechanisms in existing catalysts, but even to assist the design of new catalysts.

Herein we move the first steps in this direction by performing ab initio molecular dynamics (AIMD) simulations with a biasing potential[16] to study mono-Ru catalysts of the type $[(Ar)Ru(X)(bpy)]^+$. Indeed this class of novel mono-Ru catalysts and closely related Ru complexes have been recently synthesized and show water oxidation activity with high turnover numbers.[17,18] We assume a catalytic cycle as postulated for the Ir catalyst in ref. [11] where the X^- ligand is initially replaced by a water molecule. This intermediate then undergoes the first two oxidation steps in which two protons and two electrons are released yielding a formally Ru(IV)oxo complex, which is generally assumed to be the active species in the formation of the O–O bond with another water molecule. In Scheme 1 we schematically show the Ru complex and the different aromatic ligands (Ar) considered herein. Here we focus on this crucial reaction step starting from the Ru(IV)oxo intermediate and analyze possible reaction paths leading to the formation of a hydroperoxo intermediate. Most previous DFT-based investigations on similar homogeneous catalysts are performed in gas phase or with solvation effects included using continuum solvation models. Recent studies have underlined

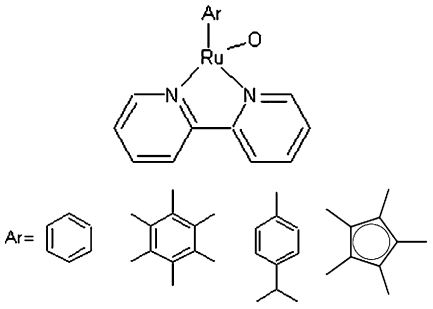

Scheme 1. Mononuclear Ru catalyst. The aromatic ligands (Ar) are, from left to right, benzene, hexamethylbenzene, cymene, and pentamethylcyclopentadienyl (Cp*).

[a] J. L. Vallés-Pardo, M. C. Guijt, Dr. K. S. Joya, Prof. Dr. H. J. M. de Groot, Dr. F. Buda
Leiden Institute of Chemistry
Leiden University
P.O. Box 9502, 2300 RA Leiden (The Netherlands)
E-mail: f.buda@chem.leidenuniv.nl

[b] Dr. M. Iannuzzi
Institute of Physical Chemistry
Universität Zürich
Winterthurerstrasse 190, CH-8057 (Zürich)

[c] Dr. K. S. Joya
Department of Chemistry
University of Engineering and Technology
GT Road, 54890, Lahore, Punjab (Pakistan)

the importance of adding explicit water molecules as they can have a direct role in the reaction mechanism.[19,20] Herein we include dynamic effects and an explicit solvent environment to provide a more realistic description of the process.

2. Results and Discussion

2.1. Characterization of the $[(Ar)Ru(O)(bpy)]^{+2}$ Intermediate

We first investigate the Ru(IV)oxo complex that is assumed to be the active species in the O–O bond formation. The initial geometry has been generated starting from the DFT-optimized coordinates of the analogous Ir-based catalysts provided in ref. [11] and by substituting the Ir atom with Ru. We then optimize the geometry of the $[(Ar)Ru(O)(bpy)]^{2+}$ species with different aromatic ligands and for different spin states using several functionals. The inclusion of van der Waals corrections is crucial for the structural stability of the complex, as without these corrections the Ru–Ar bond breaks during the geometry optimization. Table 1 shows the comparison of the relative energies for different possible multiplicities. We notice that all the functionals, both hybrid and non-hybrid, consistently give the same lowest-energy spin state. In particular, the triplet is the ground state for the benzene and hexamethylbenzene ligands, while the doublet is the ground state for the complex with the Cp* ligand. We can also observe quantitative differences between the hybrid and non-hybrid functionals, with the latter usually giving a smaller energy splitting between the two lowest states compared to the hybrid functionals. Given that all functionals considered here provide consistent results, we use the OPBE functional for the subsequent AIMD simulations mostly for computational efficiency (see also the Computational Method and Details section).

Table 1. Comparison of the energies of the $[(Ar)Ru(O)(bpy)]^{2+}$ for different multiplicities and calculated using various functionals. The values are given in kcal mol^{-1} and are relative to the lowest-energy spin state.

Benzene	BLYP	OPBE	B3LYP	B3LYP*
Triplet	0	0	0	0
Singlet	3.5	6.5	13.9	13.2
Quintet	24.3	89.7	47.0	48.0
Hexamethylbenzene	**BLYP**	**OPBE**	**B3LYP**	**B3LYP***
Triplet	0	0	0	0
Quintet	16.4	44.0	9.7	10.4
Singlet	224.0	7.6	20.3	19.7
Cp*	**BLYP**	**OPBE**	**B3LYP**	**B3LYP***
Doublet	0	0	0	0
Quartet	22.9	22.6	29.7	29.5
Sextet	84.0	87.2	106.1	102.0

In Table 2 we show a few relevant geometrical parameters and effective RESP atomic charges[21] obtained for the most stable multiplicity using the OPBE functional. These results show the effect of using different aromatic ligands on the geometric and electronic structure of the catalyst. It appears that the distance between the ruthenium and the oxo ligand (Ru–O) is not strongly affected by the choice of the aromatic ring. We also report the average value of the two distances between the ruthenium and the nitrogen atoms of the bipyridine (Ru–N). The distance between ruthenium and the centre of the aromatic ring (Ru–Ar) is also an interesting parameter since a weak interaction between them could be a source of instability in the catalyst. This distance becomes shorter for increasing ring size. The effective RESP charges for ruthenium, oxygen and the aromatic ring are quite sensitive to the choice of the ligand. Specifically, the oxo ligand carries a negative charge, which increases for aromatic rings richer in electrons.

Table 2. Geometrical parameters and effective RESP atomic charges for the $[(Ar)Ru(O)(bpy)]^{2+}$ complex using different aromatic rings. These results are obtained with the OPBE functional for the lowest energy spin state. Distances are given in Å, angles in degrees.

Geometrical parameters	Ru–O	Ru–Ar	Ru–N	O–Ru–Ar
Benzene	1.74	1.90	2.11	125.88
Hexamethylbenzene	1.73	1.80	2.25	123.87
Cp*	1.71	1.86	2.03	136.04
Effective RESP charges				
	Ru	O	Ar	
Benzene	1.86	−0.45	0.30	
Hexamethylbenzene	3.62	−1.10	0.57	
Cp*	3.45	−1.22	0.19	

In Figure 1 we show the spin density for the $[(benzene)Ru(O)(bpy)]^{2+}$ complex in the triplet state, clearly pointing to a strong radical character of the oxo ligand, which we would then indicate in the following as the oxyl radical. This radical character has been considered as a key feature to activate the O–O bond formation.[22]

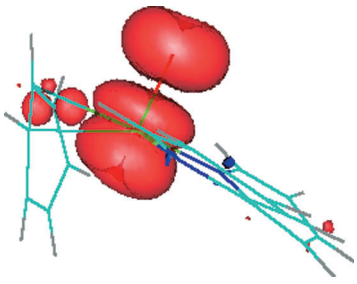

Figure 1. Spin-density isosurface for the $[(benzene)Ru(O)(bpy)]^{2+}$ in the triplet state. This was produced with gOpenMol.

2.2. AIMD simulations for the O–O bond formation

In this section we investigate two different reaction mechanisms for O–O bond formation using metadynamics simulations, as described in the computational method section. In the first scenario we assume that the incoming water molecule

first coordinates to the Ru, thus creating a heptacoordinated intermediate, followed by a second step in which the O–O bond could be formed. In the second case we consider that the incoming water molecule attacks the oxyl radical for a direct O–O reaction. These two suggested pathways are similar to those addressed in a recent theoretical study on ruthenium water oxidation catalysts.[14]

In order to assess the importance of the inclusion of an extensive solvation at the quantum-mechanical level, we perform metadynamics simulations for the $[(benzene)Ru(O)(bpy)]^{+2}$ catalyst both in vacuum and in an explicit solvent environment. For the simulations in vacuum we take as starting geometry the optimized Ru complex plus three water molecules in its proximity (see Figure 2). For the simulations in the presence of an explicit solvent environment we include in our molecular dynamics box the catalyst plus 73 water molecules with periodic boundary conditions (also see the Computational Method and Details section).

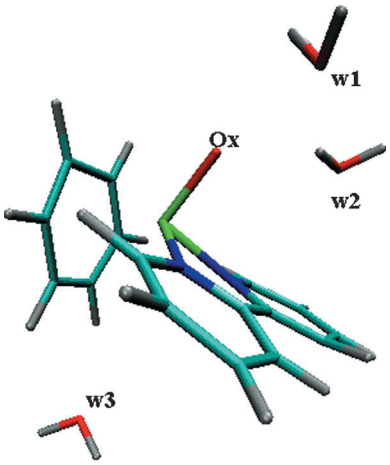

Figure 2. Optimized geometry of the $[(benzene)Ru(O)(bpy)]^{2+}$ intermediate including three water molecules. This image was made with VMD.[48]

2.3. Ru-Ow3 Approach

In the first AIMD simulation for this approach we include the $[(Benzene)Ru(O)(bpy)]^{+2}$ complex plus three water molecules: w1 and w2 close to the oxyl radical and w3 at 3.5 Å from the ruthenium atom on the opposite side (Figure 2). The collective variable (CV) used in this simulation is the Ru–Ow3 distance with a maximum allowed value of 3.7 Å. In Figure 3 we show the Ru–Ow3 and the Ru–benzene distances along the AIMD trajectory. We observe that the benzene breaks its coordination bond when the incoming water enters the coordination shell of the metal (Ru–Ow3 $\approx$ 2.7 Å), suggesting that this pathway is unfeasible. We should point out that we continue to build up the biasing potential even when the water is coordinated to the Ru (see Figure 3, after about 1 ps). This is why the water eventually leaves the Ru coordination shell in the second part of the trajectory.

In order to check if the observed structural instability of the catalyst is related to the specific choice of the aromatic ligand,

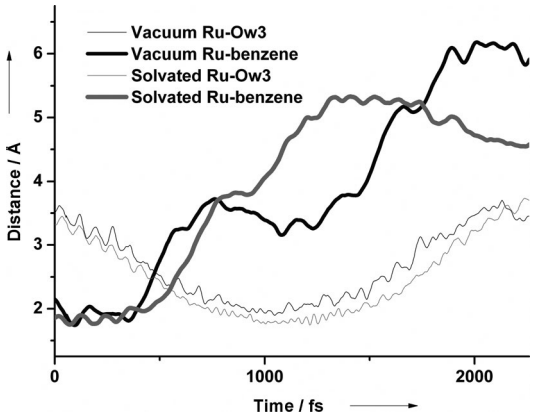

Figure 3. Relevant geometrical parameters along the metadynamics simulation of the $[(benzene)Ru(O)(bpy)]^{2+}$ complex, in which the Ru–Ow3 distance is the collective variable. For the atomic labeling in the legend, please refer to Figure 2.

or to the missing water environment, we perform additional simulations using the same setup. First we substitute the benzene ligand with hexamethylbenzene and cymene and analyze the same reaction path in vacuum. Furthermore we consider again the case of benzene but in a water-solvated environment. In all these simulations we observe a similar behaviour with the aromatic ligand leaving the coordination shell of the metal. In Figure 3 we show for comparison the results for benzene obtained in vacuum and in the solvated environment. We can see that the degradation of the catalyst is very similar in both cases, with the water environment only slightly slowing down the process. We can then conclude that the heptacoordinated form of the Ruthenium (assuming that these aromatic rings are treated as tridentate ligands) is not stable for this class of catalysts.

2.4. Ox–Ow1 Approach

The starting geometry for these metadynamics simulations is the same as used in the previous case (Figure 2), but here the CV is the distance between the oxyl radical and the oxygen of water w1 (Ox–Ow1) with an initial value of 3.5 Å and a maximum allowed value of 3.7 Å. The results for the simulation in vacuum are shown in Figure 4.

We can observe that when the Ox–Ow1 distance becomes smaller than ~1.8 Å, at the same time an increase of the Ru–Ox and of the Hw1–Ow1 distances occurs. This observation is in line with the expectation. When the bond between Ox and Ow has been created, the interaction between Ruthenium and the oxyl radical becomes weaker since the double bond character is lost. On the other hand we also expect that the O–O bond formation would be accompanied by a proton jump from the reactant water, thus this slight increase of the Hw1–Ow1 distance can be interpreted as an attempt of a proton jump. It is clear that we are still missing a proper proton acceptor in this simulation.

In order to address the question about the importance of the solvent environment for this reaction, we perform the

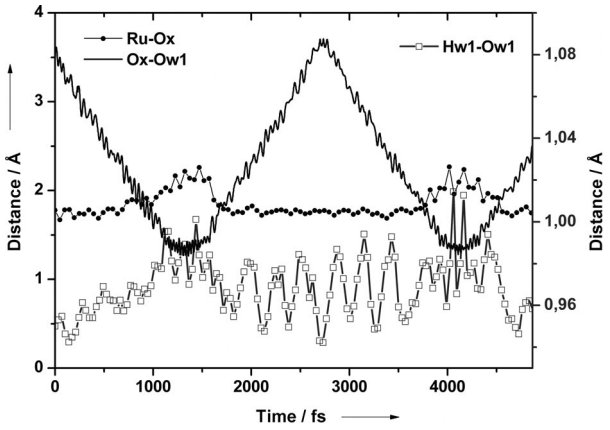

Figure 4. Relevant geometrical parameters along the metadynamics simulation of the $[(benzene)Ru(O)(bpy)]^{2+}$ in gas phase, in which the Ox–Ow1 distance is the collective variable. For the atomic labeling in the legend, please refer to Figure 2. The right axis refers to the Hw1–Ow1 distance (line with open squares).

same metadynamics simulation in the presence of explicit water molecules surrounding the catalyst (see the Computational Method and Details section). The results are illustrated in Figure 5, where we plot the relevant geometrical parameters describing the reaction. We should again emphasize that only the distance between the oxygen of the water molecule (Ow1) and the oxyl radical (Ox–Ow1, dark solid line) is driven by the adaptive biasing potential, while all other structural changes occur spontaneously. When Ox–Ow1 is about 1.8 Å we observe an increase in the Ru-Ox distance (line with dots) and an increase in the water bond length Hw1–Ow1 (line with open squares), similarly to the result of the previously described simulation in vacuum. However, now we also observe a decrease in the distance between Hw1 and the oxygen of a second water molecule (Hw1–Ow2, light solid line). Soon after the Ox-Ow1 distance has reached a value of ~1.4 Å, indicating the formation of the O–O bond, one proton of the reactant water jumps on the second water, thus forming a hydronium ion

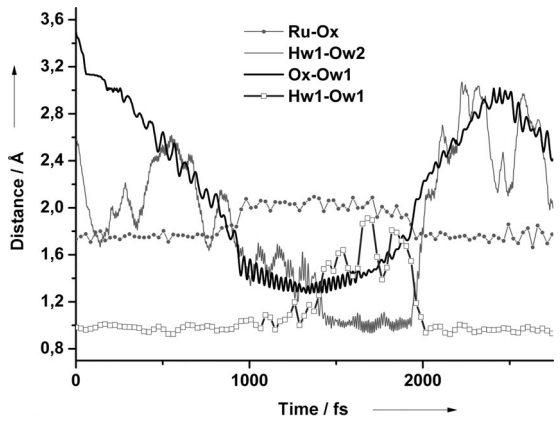

Figure 5. Relevant geometrical parameters along the metadynamics simulation of the solvated $[Ru(Benzene)(bpy)(O)]^{2+}$ complex, in which the Ox–Ow1 distance is the collective variable. For the atomic labeling in the legend, please refer to Figure 2.

OH_3^+. In Figure 6, a snapshot of the simulation after 1.7 ps, clearly shows the formation of the Ru-OOH intermediate and of a hydronium ion. In Figure 5 we can also see that if we continue the metadynamics simulation, the biasing potential will fill the local minimum in the free energy landscape corresponding to this intermediate state and the reaction is reversed.

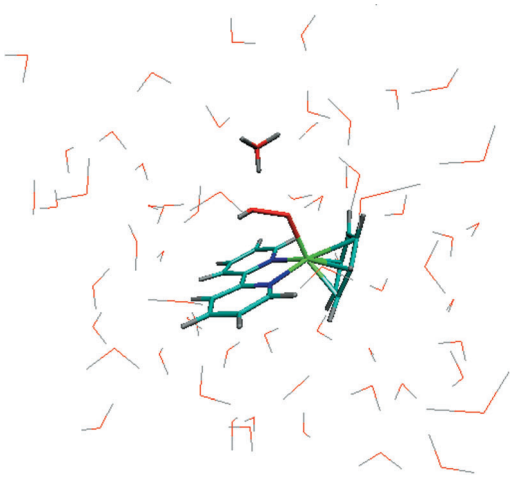

Figure 6. Hydroperoxo intermediate in solvated environment. The hydronium ion formed in the simulation is also highlighted. This snapshot is taken after 1.7 ps of simulation. This image was made with VMD.[48]

For an estimate of the free-energy profile we use a thermodynamic integration technique with constrained MD, in which each initial configuration is extracted from the metadynamics trajectory. The preliminary estimated free-energy shows a low activation barrier of around 10 kcal mol^{-1} and a $\Delta G \approx -10$ kcal mol^{-1} between the Ru–OOH intermediate and the initial complex, indicating that this reaction step is exothermic. The transition state is found for a Ox–Ow1 distance between 1.85 and 1.95 Å. A full report of these simulations will be presented elsewhere. Here we mention that from our constrained AIMD simulations we observe that the proton jumps spontaneously to the water environment when the Ox–Ow1 distance is shorter than the transition state value. Moreover, we never observe the oxo ligand acting as proton acceptor, as suggested in ref. [11]. We also perform two additional AIMD simulations of few ps at room temperature without constraints for the solvated initial Ru-oxyl and the final Ru-hydroperoxo intermediates and verify that indeed these two intermediates are stable in water.

2.5. Characterization of the $[(benzene)Ru(OOH)(bpy)]^{+1}$ Intermediate and the Transition State

In this section we analyze the structural and electronic properties of the Ru–OOH intermediate and the transition state found in the AIMD simulations. In Table 3 we present a comparison between geometrical parameters and relative energies obtained in the gas phase. For a proper energetic comparison

Table 3. Comparison between the energy in vacuum of initial complex (Ru–oxyl) including two water molecules, transition state (TS) and final intermediate including the hydronium (Ru–HOOH). Geometrical parameters for the hydroperoxo complex (Ru–OOH) are also reported. Distances are in Å and energy in kcal mol^{-1}. For the atomic labeling, please refer to Figure 2. The lowest-energy multiplicity is indicated.

	Ru–Ox	Ru–Benzene	Ox–Ow1	Relative energy	Multiplicity
Ru–oxyl	1.75	1.77	3.08	0	Triplet
TS	1.80	1.72	1.93	24.3	Singlet
Ru-HOOH	2.20	1.63	1.43	11.0	Singlet
Ru–OOH	2.00	1.63	1.43	–	Singlet

we consider the same cubic simulation box size, with a side length of 18 Å, for each supramolecular complex. Both the initial complex (Ru-oxyl) and the transition state (TS) include two water molecules, while for the hydroperoxo intermediate we include the hydronium cation. In this way in each calculation we have the same number of atoms and total charge.

There are a few important considerations emerging from this analysis. First, we notice that during the oxygen bond formation (Ox–Ow1) the Ru–Ox distance increases as expected, while the Ru–benzene distance decreases. During the geometry optimization of the Ru–OOH complex with the hydronium cation, we observe that one proton is transferred from the hydronium to the Ox forming a hydrogen peroxide ligand (Ru–HOOH). This final complex resembles closely that found in the case of the similar Ir catalyst studied in ref. [11]. This result is at variance with the behavior observed in the AIMD simulations in water where the hydronium is stabilized by the solvation shell, underlining the importance of the solvent environment.

A preliminary characterization of the transition state in vacuum including the reactant water and the water accepting the proton is shown in Figure 7 and some of the corresponding geometrical parameters are given in Table 3. In particular we find d(Ox–Ow1) = 1.93 Å and that the second water (w2) is ready to accept the proton with d(Ow2–Hw1) = 1.57 Å. The TS energy is about 24 kcal mol^{-1} higher than the reactant, a value which is similar to that found by Blakemore et al. for the analogous Ir catalyst when they include two water molecules.[11] However, the transition state found for the Ir complex has a distance d(Ox–Ow1) = 1.50 Å, which is much shorter than in our system and very close to the equilibrium O–O distance in the hydroperoxo intermediate. We actually find another transition state with a similar Ox–Ow1 short distance that according to the vibrational analysis corresponds to the proton transfer step from the reactant water to the second water and is not representative of the actual transition state for the O–O bond formation. From the comparison with the free-energy barrier estimated in the water environment, we can also conclude that this solvent is important in facilitating this reaction step. The energy difference between the initial and the final complex in vacuum cannot be directly compared with the result in water since we obtain two different intermediates. Therefore the results obtained with an explicit solvent are not only quantitatively but also qualitatively different from those obtained in the gas phase.

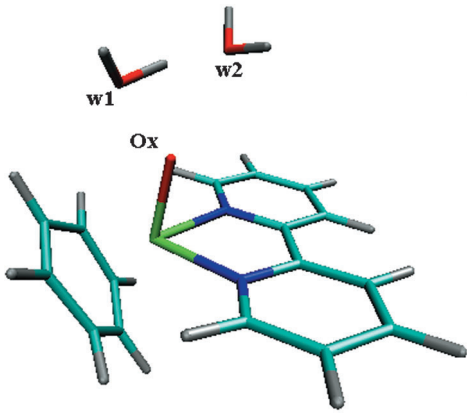

Figure 7. Transition state structure of the Ru catalyst with benzene ligand including two water molecules. This image was made with VMD.[48]

Another point that is usually discussed in the literature for this class of catalysts is the oxidation state of the metallic centres. To check if the Ru atom increases or decreases its oxidation state during this reaction step, we perform a RESP charge analysis of the optimized initial (Ru–oxyl) and final (Ru–OOH) intermediate states in gas phase. This analysis clearly shows that the ruthenium increases its positive charge in spite of the fact that the overall charge of the hydroperoxo intermediate decreases to +1. This excess of positive charge on the Ru is overcompensated by an increase in the negative charge located mostly in the benzene and in the bipyridine ligands. This increased charge polarization in the complex can explain the shortening of the Ru–benzene distance due to a stronger electrostatic interaction.

Finally, in Table 3 we also report the most stable spin multiplicity for the hydroperoxo intermediate, which turns out to be a singlet unlike the initial complex where we found a triplet state. Therefore, our results point to the occurrence of a spin-crossover during the reaction. This spin-crossover appears to be located at (or close to) the transition state, where we find that the singlet and triplet states differ in energy by only ~1 kcal mol^{-1}. This result is reminiscent of the two-state reactivity discussed by Shaik and coworkers for Fe complexes.[23]

3. Conclusions

Herein we have shown that the ab initio molecular dynamics approach with an adaptive biasing potential can be an important tool to efficiently explore several potential reaction paths for water oxidation reactions at room temperature and with an explicit inclusion of the water environment. We have focused our analysis to a class of mononuclear ruthenium catalysts which are inspired by recently synthesized analogous iridium-based catalysts. In the computer simulations is easy to check the effect of modifying the ligands and/or the metal centers and therefore this type of in silico studies can be used to assist

the development of new efficient and robust catalysts for artificial photosynthesis.

We find that the reaction path involving first a coordination step of the reactant water to the metal center is not viable since it leads to a structural instability of the catalyst with the breaking of the metal-aromatic ligand coordination bond. The alternative path, in which the reactant water directly attacks the oxyl radical, leads to the formation of the O–O bond resulting in a Ru-hydroperoxo complex and to the release of one proton into the solvent environment. This simulation shows that the proton release occurs spontaneously at room temperature and thus is not the rate-limiting step. Moreover, it underlines the crucial role played by the solvent in facilitating the formation of the hydroperoxo intermediate with an activation free energy of only about 10 kcal mol^{-1}. From the analysis of the charge distribution in the complex before and after the reaction, we can interpret this step in the catalytic cycle as a proton-coupled electron transfer (PCET) process, since electron charge moves from the metallic center to the aromatic ring. We suggest that the aromatic ligand can play the role of an electron charge buffer facilitating the electron steps in the catalytic cycle. Interestingly, a spin-crossover appears to occur along this reaction path since the final intermediate is found to be a singlet while the initial Ru-oxyl complex is a triplet state. Further investigations are ongoing to get a more accurate estimate of the free energy profile and the effect of different aromatic ligands.

Computational Method and Details

The ab initio molecular dynamics (AIMD) simulations[24] herein are performed with the CP2K program.[25] We use the OPBE exchange–correlation functional for the DFT electronic structure calculations.[26] The choice of this non-hybrid functional is mainly dictated by the computational efficiency in the AIMD and is justified by previous work where it has been shown to give an accurate description of several transition metal complexes.[27–30] Here we perform additional tests to validate the OPBE results using the non-hybrid functional BLYP[31,32] and the hybrid functionals B3LYP and B3LYP*, which differ for the amount of exact exchange (0.2 and 0.15, respectively) and are usually considered more reliable for these systems.[32,33] The ADF program is used for the calculations with the hybrid functionals.[34,35] The CP2K program employs a mixed basis set approach with Gaussian-type orbitals (GTO) and plane waves (PWs).[36] GTO functions are used to expand the molecular orbitals and the charge density in real space, whereas PWs are used for the representation of the charge density in reciprocal space. An energy cut-off of 280 Ry is used for the plane-waves basis set. The TZVP-MOLOPT-GTH[37] Gaussian basis set is chosen for all the atoms in the catalyst except ruthenium for which a DZVP-MOLOPT-GTH is used. The water molecules close to the catalyst and involved in the reaction are treated at the TZVP-MOLOPT-GTH level, whereas the DZVP-MOLOPT-GTH is used for all the other water molecules. We use pseudopotentials of the GTH form for all the elements.[38–40] The pseudopotential for Ru is generated with 16 valence electrons. In the ADF calculations a TZP Slater type basis set is used.

Due to the presence of π–cation interactions between the metallic centre and the aromatic ligand, it is crucial to include van der Waals corrections. In all the AIMD simulations the DFT-D2 van der Waals correction by Grimme is applied.[41,42] Specifically, we use the PBE parameters for the OPBE calculations and the corresponding parameters for the other functionals used. Periodic boundary conditions (PBC) are applied in the simulations with explicit solvent, while for the gas phase simulations without PBC the Martina–Tuckerman approach is used for the Poisson solver.[43] For the AIMD simulations we use a time step $\Delta t = 0.5$ fs. In order to efficiently explore possible reaction pathways, we use the metadynamics approach proposed by Laio and Parrinello,[16] which is efficiently implemented in the CP2K code. The metadynamics is a coarse-grained dynamics on the free-energy surface (FES) defined by a few collective variables (e.g. the distance between two atoms) using an adaptive bias potential in order to escape from a local minimum. At each metadynamics step the evolution of the collective variables is guided by a generalized force which combines the action of the thermodynamic force, that would trap the system in a free energy minimum, and a history-dependent force which disfavours configurations already visited. This history-dependent potential is built as a sum of Gaussian functions centered in the explored values of the collective variables. The height and the width of the Gaussian are 10^{-3} Hartree and 0.02 a.u., respectively. In our simulations we evolve the collective variables with one metadynamics step every 20 AIMD time steps. In this way we can quickly explore the reaction pathway, but we sacrifice the accuracy of the free-energy surface along the collective variable. For a preliminary estimate of the free-energy we instead use here a thermodynamic integration technique with constrained MD.[44,45] We consider six points along the Ox–Ow distance in the range 1.45–2.25 Å and for each point we equilibrate the system for about 1.5 ps. We find this combination of the metadynamics approach and constrained MD computationally more efficient in this case.

For a more realistic study of the reaction we include explicitly the solvent environment. Solvated simulations are performed in an orthorhombic box of $16 \times 15.5 \times 15$ Å^3 containing the Ru catalyst and 73 water molecules, which are all treated at the quantum-mechanical level. Before starting the AIMD simulations, the solvent is equilibrated with force field MD simulations while keeping the transition metal complex fixed. First the volume of the box is adjusted with a constant pressure simulation and then the system is further equilibrated at constant volume and constant room temperature. For these preliminary steps the Discovery Studio software[46] is used with the CHARMM force field and the TIP3P model.[47]

Acknowledgements

The use of supercomputer facilities was sponsored by The Netherlands National Computing Facilities Foundation (NCF), with financial support from the Netherlands Organization for Scientific Research (NWO).

Keywords: ab initio calculations · density functional calculations · molecular dynamics · ruthenium catalysts · water splitting

[1] W. Lubitz, E. J. Reijerse, J. Messinger, *Energy Environ. Sci.* **2008**, *1*, 15 – 31.
[2] E. M. Sproviero, J. A. Gascón, J. P. McEvoy, G. W. Brudvig, V. S. Batista, *J. Am. Chem. Soc.* **2008**, *130*, 3428 – 3442.
[3] P. E. M. Siegbahn, *J. Photochem. Photobiol. B* **2011**, *104*, 94 – 99.
[4] Y. Xu, T. Åkkerman, V. Gyollai, D. Zou, L. Eriksson, L. Duan, R. Zhang, B. Åkkerman, L. Sun, *Inorg. Chem.* **2009**, *48*, 2717 – 2719.
[5] D. J. Wasylenko, C. Ganesamoorthy, B. D. Koivisto, M. A. Henderson, C. P. Berlinguette, *Inorg. Chem.* **2010**, *49*, 2202 – 2209.
[6] M. W. Kanan, D. G. Nocera, *Science* **2008**, *321*, 1072 – 1075.

[7] F. Jiao, H. Frei, *Angew. Chem.* **2009**, *121*, 1873 – 1876; *Angew. Chem. Int. Ed.* **2009**, *48*, 1841 – 1844.
[8] Q. Yin, J. M. Tan, C. Bresson, Y. V. Geletii, D. G. Musaev, A. E. Kuznetsov, Z. Lou, K. I. Hardcastle, C. L. Hill, *Science* **2010**, *328*, 342 – 345.
[9] N. D. McDaniel, F. J. Coughlin, L. t. Tinker, S. Bernard, *J. Am. Chem. Soc.* **2008**, *130*, 210 – 217.
[10] J. F. Hull, D. Balcells, J. D. Blakemore, C. D. Incarvito, O. Eisenstein, G. W. Brudvig, R. H. Crabtree, *J. Am. Chem. Soc.* **2009**, *131*, 8730 – 8731.
[11] J. D. Blakemore, N. D. Schley, D. Balcells, J. F. Hull, G. W. Olack, C. D. Incarvito, O. Eisenstein, G. W. Brudvig, R. H. Crabtree, *J. Am. Chem. Soc.* **2010**, *132*, 16017 – 16029.
[12] A. Savini, G. Bellachioma, G. Ciancaleoni, C. Zuccaccia, D. Zuccaccia, A. Macchioni, *Chem. Commun.* **2010**, *46*, 9218 – 9219.
[13] D. E. Polyansky, J. T. Muckerman, J. Rochford, R. Zong, R. P. Thummel, E. Fujita, *J. Am. Chem. Soc.* **2011**, *133*, 14649 – 14665.
[14] L. P. Wang, Q. Wu, T. Van Voorhis, *Inorg. Chem.* **2010**, *49*, 4543 – 4553.
[15] T. Wang, G. W. Brudvig, V. S. Batista, *J. Chem. Theory Comput.* **2010**, *6*, 2395 – 2401.
[16] A. Laio, M. Parrinello, *Proc. Natl. Acad. Sci. USA* **2002**, *99*, 12562 – 12566.
[17] a) K. S. Joya, H. J. M. de Groot, Metal complex and use as multi-electron catalyst. Netherlands Patent Application no. 2005512, Oct, **2010**; (submitted); b) K. S. Joya, H. J. M. de Groot, Metal complex and use as multi-electron catalyst. International Patent Application no. PCT/NL2011/050673, Oct, **2011**, *submitted*.
[18] L. Bernet, R. Lalrempuia, W. Ghattas, H. Mueller-Bunz, L. Vigara, A. Llobet, M. Albrecht, *Chem. Commun.* **2011**, *47*, 8058 – 8060.
[19] F. Bozoglian, S. Romain, M. Z. Ertem, T. K. Todorova, C. Sens, J. Mola, M. Rodríguez, I. Romero, J. Benet-Buchholz, X. Fontrodona, C. J. Cramer, L. Gagliardi, A. Llobet, *J. Am. Chem. Soc.* **2009**, *131*, 15176 – 15187.
[20] X. Sala, M. Z. Ertem, L. Vigara, T. K. Todorova, W. Chen, R. C. Rocha, F. Aquilante, C. J. Cramer, L. Gagliardi, A. Llobet, *Angew. Chem.* **2010**, *122*, 7911 – 7913; *Angew. Chem. Int. Ed.* **2010**, *49*, 7745 – 7747.
[21] A. Laio, F. L. Gervasio, J. VandeVondele, M. Sulpizi, U. Rothlisberger, *J. Phys. Chem. B* **2004**, *108*, 7963 – 7968.
[22] M. Lundberg, M. R. A. Blomberg, P. E. M. Siegbahn, *Inorg. Chem.* **2004**, *43*, 264 – 274.
[23] S. Shaik, S. P. de Visser, F. Ogliaro, H. Schwarz, D. Schröder, *Curr. Opin. Chem. Biol.* **2002**, *6*, 556 – 567.
[24] D. Marx, J. Hutter, *Ab Initio Molecular Dynamics: Basic Theory and Advanced Methods*, Cambridge University Press, Cambridge, **2009**.
[25] The CP2K developers group. http://cp2k.berlios.de/.
[26] M. Swart, A. W. Ehlers, K. Lammertsma, *Molec. Phys.* **2004**, *102*, 2467 – 2474.
[27] A. R. Groenhof, A. W. Ehlers, K. Lammertsma, *J. Am. Chem. Soc.* **2007**, *129*, 6204 – 6209.
[28] M.-S. Liao, J. D. Watts, M.-J. Huang, *J. Phys. Chem. A* **2007**, *111*, 5927 – 5935.
[29] J. Conradie, A. Ghosh, *J. Chem. Theory Comput.* **2007**, *3*, 689 – 702.
[30] M. Swart, *J. Chem. Theory Comput.* **2008**, *4*, 2057 – 2066.
[31] A. D. Becke, *Phys. Rev. A* **1988**, *38*, 3098 – 3100.
[32] C. T. Lee, W. T. Yang, R. G. Parr, *Phys. Rev. B* **1988**, *37*, 785 – 789.
[33] A. D. Becke, *J. Chem. Phys.* **1993**, *98*, 5648 – 5652.
[34] G. te Velde, F. M. Bickelhaupt, S. J. A. van Gisbergen, C. Fonseca Guerra, E. J. Baerends, J. G. Snijders, T. Ziegler, *J. Comput. Chem.* **2001**, *22*, 931 – 967.
[35] ADF2009.01, SCM, Theoretical Chemistry, Vrije Universiteit, Amsterdam, The Netherlands, http://www.scm.com/.
[36] J. VandeVondele, M. Krack, F. Mohamed, M. Parrinello, T. Chassaing, J. Hutter, *Comput. Phys. Commun.* **2005**, *167*, 103 – 128.
[37] J. VandeVondele, J. Hutter, *J. Chem. Phys.* **2007**, *127*, 114105 – 114113.
[38] S. Goedecker, M. Teter, J. Hutter, *Phys. Rev. B* **1996**, *54*, 1703 – 1710.
[39] C. Hartwigsen, S. Goedecker, J. Hutter, *Phys. Rev. B* **1998**, *58*, 3641 – 3662.
[40] M. Krack, *Theor. Chem. Acc.* **2005**, *114*, 145 – 152.
[41] S. Grimme, *J. Comput. Chem.* **2006**, *27*, 1787 – 1799.
[42] S. Grimme, J. Antony, S. Ehrlich, H. Krieg, *J. Chem. Phys.* **2010**, *132*, 154104.
[43] G. J. Martyna, M. E. Tuckerman, *J. Chem. Phys.* **1999**, *110*, 2810 – 2821.
[44] M. Sprik, G. Ciccotti, *J. Chem. Phys.* **1998**, *109*, 7737 – 7744.
[45] W. K. den Otter, W. J. Briels, *J. Chem. Phys.* **1998**, *109*, 4139 – 4146.
[46] Accelrys Software Inc., *Discovery Studio Modeling Environment* http://accelrys.com/.
[47] A. D. MacKerell, Jr., D. Bashford, M. Bellott, R. L. Dunbrack, Jr., J. D. Evanseck, M. J. Field, S. Fischer, J. Gao, H. Guo, S. Ha, D. Joseph-McCarthy, L. Kuchnir, K. Kuczera, F. T. K. Lau, C. Mattos, S. Michnick, T. Ngo, D. T. Nguyen, B. Prodhom, W. E. Reiher III, B. Roux, M. Schlenkrich, J. C. Smith, R. Stote, J. Straub, M. Watanabe, J. Wiórkiewicz-Kuczera, D. Yin, M. Karplus, *J. Phys. Chem. B* **1998**, *102*, 3586 – 3616.
[48] VMD is developed with NIH support by the Theoretical and Computational Biophysics group at the Beckman Institute, University of Illinois at Urbana-Champaign. (http://www.ks.uiuc.edu/Research/vmd/).

Received: July 15, 2011
Revised: December 13, 2011
Published online on December 28, 2011

